



Thermal conductivity of MgO periclase at high pressure: Implications for the D'' region

Nico de Koker*

Bayerisches Geoinstitut, Universität Bayreuth, Germany

ARTICLE INFO

Article history:

Received 15 December 2009
Received in revised form 4 February 2010
Accepted 5 February 2010
Available online 4 March 2010

Editor: R.W. Carlson

Keywords:

thermal conductivity
core–mantle boundary
heat flux
periclase
Earth's mantle

ABSTRACT

The thermal conductivity of the lowermost mantle determines the rate at which heat flows across the core–mantle boundary, and consequently plays a central role in the thermal evolution of both the mantle as well as the core. In an effort to test and improve model estimates of thermal conductivity in the deep mantle, we perform first-principles computations of the lattice conductivity for MgO periclase. The method uses the Peierls–Boltzmann transport equation via a combination of first-principles molecular dynamics and first-principles lattice dynamics. Phonon lifetimes are found to be inversely proportional to temperature, and increases 3-fold as the density is increased from 3.37 to 5.49 g/cm³. Thermal conductivities increase nearly 6-fold over the same density interval, and show excellent agreement with the available experimental measurements. We use these results to assess how conductivity measurements of mantle minerals can be reliably extrapolated to conditions characteristic of the lowermost mantle, and find Debye theory to be superior for this task. We then apply this insight to estimate the conductivity of MgSiO₃ perovskite in the lowermost mantle, and combine this with our computational results for MgO periclase to construct a model estimate for a representative lower mantle assemblage. We find the mantle conductivity to be 5.9 ± 0.6 W/m K at the top of the thermal boundary layer and 4.0 ± 0.5 W/m K at its base, implying core–mantle boundary heat flux values at the lower end of geophysical estimates.

© 2010 Elsevier B.V. All rights reserved.

1. Introduction

Large scale dynamics within the Earth is the result of its ongoing attempt to cool down. Heat is transported towards the surface by large scale convection in the mantle and in the core, and by conduction across the thermal boundary layers at the core–mantle boundary and the lithosphere. Insight into the thermal transport properties of candidate lower mantle phases is vital for a detailed understanding of these processes. The thermal conductivity of the lower mantle is geophysically important for two reasons. Firstly, it determines the degree of heat flux across the core–mantle boundary, thus controlling the thermal evolution of the core and consequently the generation of the magnetic field (e.g. Sakuraba and Roberts, 2009; Buffett, 2009; Davies, 2007; Labrosse, 2003; Buffett et al., 1992). Secondly it sets the balance between conduction and convection, thus determining the convective regime (e.g. Schubert et al., 2001; Zhong, 2006).

Seismic studies have shown that the core–mantle boundary region is laterally heterogeneous with likely variations in temperature, composition and heat flux (e.g. Lay et al., 1998). Two large low seismic velocity regions extending to shallower lower mantle depths have

been observed in seismic tomography models, and are proposed to be intimately associated with the generation of mantle plumes (Burke et al., 2008). Plausible variations in temperature and chemistry at the base of the mantle are compatible with the presence of both post-perovskite lenses (e.g. Hernlund et al., 2005; Buffett, 2007) and regions of partial melt (Stixrude et al., 2009; Williams and Garnero, 1996). In the light of these complexities, obtaining an accurate estimate of heat flux across the core–mantle boundary is not trivial, requiring detailed knowledge of the thermal transport properties of the candidate lowermost mantle minerals as a function of pressure, temperature, as well as composition.

Estimates for the thermal conductivity (κ) in the lower mantle range between 4 and 16 W/m K (Goncharov et al., 2009; Lay et al., 2008; Hofmeister, 2007; Hofmeister, 1999; Brown, 1986; Kieffer, 1976). The large uncertainty results mainly from two factors. Firstly, measurements of κ at high pressure are extremely challenging and often mutually inconsistent, causing notable uncertainties even at upper mantle pressures that are amplified upon extrapolation to the conditions of the lowermost mantle. Secondly, there is little consensus on how to represent the pressure dependence of κ ; different models yield very different extrapolations (Goncharov et al., 2009; Hofmeister, 2007; Brown, 1986). Due to the large uncertainties and a relatively small pressure range in the experimental data, distinguishing among these various models was not previously possible.

* Tel.: +49 921 55 3745; fax: +49 921 55 3769.
E-mail address: nico.dekoker@uni-bayreuth.de.

First-principles methods present an ideal solution to this problem, as they are equally accurate and robust at ambient and high pressures. We have recently implemented a simple and efficient method for computing thermal conductivity from first principles (de Koker, 2009), with low pressure \mathcal{K} values for MgO periclase obtained by this method in close agreement with experiment. Here we apply this method to compute \mathcal{K} for MgO over a range of pressures relevant to the entire mantle. Using these results, we consider the merits of the various models describing the compressional behaviour of \mathcal{K} , apply the preferred model to reassess the estimates of \mathcal{K} at the base of the mantle, and subsequently the heat flux through the core–mantle boundary.

2. Theoretical background

Conductive heat transport in solid materials can occur through migration of electrons, photons and phonons. Electronic conductivity is very important in metals, but can be neglected for mantle minerals. Radiative conductivity plays an important role at high temperatures, but the extent to which it contributes to the total conductivity of the Fe-containing aggregate of lower mantle minerals remains a matter of debate (Keppeler et al., 2008; Goncharov et al., 2008; Hofmeister and Yuen, 2007). The dominant fraction of conductive heat transport in the deep mantle occurs through lattice vibrations, i.e. by phonons.

Although finite lattice conductivity arises due to anharmonicity, atomic displacements are generally small enough that we may view the true anharmonic lattice vibrations as a perturbation of the harmonic case. It has been shown that where this approximation holds, \mathcal{K} can be represented via the Peierls–Boltzmann transport equation (Ziman, 1960; Klemens, 1958; Peierls, 1929)

$$\mathcal{K} = \sum_s^{3n} \int_{\mathbf{q}} v_{\mathbf{q},s}^2 c_{\mathbf{q},s} \tau_{\mathbf{q},s} d\mathbf{q}, \quad (1)$$

where $\tau_{\mathbf{q},s}$ is the phonon lifetime, $v_{\mathbf{q},s} = |\mathbf{v}_{\mathbf{q},s}|$ is the phonon group velocity

$$v_{\mathbf{q},s} = \frac{\partial \nu_{\mathbf{q},s}}{\partial \mathbf{q}}, \quad (2)$$

and $c_{\mathbf{q},s}$ is the mode heat capacity

$$c_{\mathbf{q},s} = \frac{k_B}{V} \frac{x^2 e^x}{(e^x - 1)^2}; \quad x = \frac{h\nu_{\mathbf{q},s}}{k_B T}, \quad (3)$$

with $\nu_{\mathbf{q},s}$ the vibrational frequency of mode s at wave vector \mathbf{q} . Therefore, the two key entities needed in order to compute \mathcal{K} via Eqs. (1)–(3) are $\tau_{\mathbf{q},s}$ and $\nu_{\mathbf{q},s}$.

De Koker (2009) implemented a computationally efficient method by which these components can be determined, by combining first-principles molecular dynamics (FPMD) and first-principles lattice dynamics (FPLD). The method is based on the insight that, within the phonon lifetime approximation, phonons can be viewed as damped harmonic oscillators. The spectral density at a given wave vector will consist of a set of peaks at the frequencies of vibration, each with a finite width directly related to the phonon lifetime. This is implemented using FPMD via the relation

$$\sum_s^{3n} \frac{2J_i(\mathbf{q}, 0) \tau_{\mathbf{q},s}}{1 + (2\pi\tau_{\mathbf{q},s}(\nu - \nu_{\mathbf{q},s}))^2} = \frac{4}{k_B T} \int_0^\infty J_i(\mathbf{q}, t) \exp(2\pi i\nu t) dt, \quad (4)$$

where $J_i(\mathbf{q}, t)$ is the wave vector dependent velocity field autocorrelation function

$$J_i(\mathbf{q}, t) = \lim_{t_0 \rightarrow \infty} \frac{1}{t_0} \int_0^{t_0} u_i(\mathbf{q}, t) u_i(\mathbf{q}, t' + t) dt', \quad (5)$$

$u_i(\mathbf{q}, t)$ being the reciprocal space representation of the l th velocity component at time t .

In order to describe the compressional behaviour of \mathcal{K} , it is useful to make the Debye approximation, within which Eq. (1) reduces to

$$\mathcal{K} = \frac{1}{3} \frac{\rho}{M} C_V v_D^2 \tau, \quad (6)$$

where v_D is the Debye sound velocity, ρ is the density and M the molar mass of the material. By solving the Boltzmann equation for an isotropic continuum, and considering the various combinations of possible three-phonon umklapp interactions, Roufosse and Klemens (1973) showed that phonon lifetimes should satisfy

$$1/\tau = ATv^2, \quad (7)$$

with A approximated as

$$A = \frac{2\sqrt{2}\pi k_B}{M^{2/3}} \frac{\gamma^2}{\rho^{1/3} v^3}, \quad (8)$$

with Grüneisen parameter $\gamma = (\partial \ln \nu / \partial \ln \rho)_T$ and k_B the Boltzmann constant. Different expressions for the prefactor have been derived, depending on the approximations made, but $A \propto \gamma^2 \rho^{-1/3} v^{-3}$ is a general result (Ross et al., 1984; Roufosse and Klemens, 1973; Julian, 1965).

As vibrational frequencies increase upon compression, group velocities (and Debye sound velocities) also increase. Therefore, with relatively moderate changes in the phonon lifetimes, the lattice conductivity is expected to increase with pressure.

From $A \propto \gamma^2 \rho^{-1/3} v^{-3}$ follows

$$\left(\frac{\partial \ln A}{\partial \ln \rho} \right)_T = -3\gamma - 2q + \frac{2}{3}, \quad (9)$$

and

$$\left(\frac{\partial \ln \tau}{\partial \ln \rho} \right)_T = \gamma + 2q - \frac{2}{3}, \quad (10)$$

with $q = -(\partial \ln \gamma / \partial \ln \rho)_T$. This predicts that the phonon lifetime will increase with compression for common values for γ and q . Defining

$$g = \left(\frac{\partial \ln \mathcal{K}}{\partial \ln \rho} \right)_T, \quad (11)$$

it follows from Eq. (6) that at high temperature

$$g = 3\gamma + 2q - \frac{1}{3}. \quad (12)$$

We represent $\gamma(\rho)$ using the finite strain based form of Stixrude and Lithgow-Bertelloni (2005)

$$\gamma = \frac{\gamma'_0 + (2\gamma'_0 + \gamma'_1)f + 2\gamma'_1 f^2}{3(2 + 2\gamma'_0 f + \gamma'_1 f^2)}, \quad (13)$$

where f is the Eulerian finite strain

$$f = \frac{1}{2} \left[\left(\frac{\rho}{\rho_0} \right)^{2/3} - 1 \right] \quad (14)$$

and γ'_0 and γ'_1 are constants with

$$\gamma_0 = \frac{1}{6} \gamma'_0; \quad q_0 = \frac{\gamma'_1 + 2\gamma'_0 - \gamma_0^2}{-3\gamma'_0}. \quad (15)$$

Eq. (13) allows q to vary with compression, giving results superior to the oft used constant- q approximation (de Koker and Stixrude, 2009; Stixrude and Lithgow-Bertelloni, 2005; Oganov and Dorogokupets, 2003; Karki et al., 2000; Anderson, 1974).

As an alternative approach to evaluate g , Hofmeister (2007) assumed the change in group velocity to follow the bulk sound velocity, and proposed that

$$g = K'_T, \quad (16)$$

where $K'_T = (\partial K_T / \partial P)_T$.

With g thus described, and the $1/T$ proportionality of κ predicted in Eq. (7), we may write

$$\kappa = \kappa_0 \left(\frac{\rho}{\rho_0} \right)^g \left(\frac{T_0}{T} \right), \quad (17)$$

with g described either in terms of γ via Eq. (12), or in terms of K'_T via Eq. (16), and being explicitly allowed to vary with ρ according to γ or K'_T .

3. First-principles calculations

The first-principles molecular dynamics (FPMD) simulation method we implement was discussed at length in our previous work (de Koker et al., 2008; de Koker and Stixrude, 2009; de Koker, 2009). Density functional theory (DFT; Hohenberg and Kohn, 1964; Kohn and Sham, 1965) based computations are performed using the VASP plane-wave code (Kresse and Furthmüller, 1996), with ultra-soft pseudopotentials (Kresse and Hafner, 1994) and the local density approximation (LDA; Ceperley and Alder, 1980). Electronic eigenvalues are evaluated at the supercell Brillouin zone center (Γ -point).

For computation of phonon lifetimes, simulations are performed in the micro-canonical ensemble (i.e. without a thermostat), and are run for at least 40,000 time steps (femtoseconds), with a total energy convergence threshold of 1×10^{-8} eV for computing the electronic ground state. Simulations are performed using a periodic $2 \times 2 \times 2$ supercell of eight conventional fcc unit cells (64 atoms) at densities of $\rho = 3.37, 3.75, 4.05, 4.46, 4.76, 5.10$ and 5.49 g/cm³. These simulations are supplemented by the previous conductivity calculation at $\rho = 3.67$ g/cm³ of de Koker (2009). At each density, simulations are performed for at least three temperatures between 500 and 3500 K. To assess finite size effects at high degrees of compression, a further simulation using a $3 \times 3 \times 3$ supercell (216 atoms) is performed at $\rho = 5.49$; a 216-atom simulation was previously performed at $\rho = 3.67$ g/cm³ by de Koker (2009). Pressure and temperature conditions in these simulations are summarized in Table 1.

Due to the size of the FPMD simulation cell, only a discreet set of wave vectors are accessible. In an $l \times m \times n$ cell, these are located at $[i/l, j/m, k/n]$, with i, j , and k integers. To access the rest of the Brillouin zone, first-principles lattice dynamics (FPLD) is used to compute harmonic phonon spectra via the finite displacement method (direct approach), as implemented in the PHONON code (Parlinski, 2008). The force constant matrix is constructed from Hellmann–Feynman forces computed as for FPMD using VASP, with a $4 \times 2 \times 2$ supercell, a $2 \times 4 \times 4$ Monkhorst and Pack (1976) \mathbf{k} -point grid, and a 600 eV plane-wave energy cutoff. Values for the static dielectric constant ϵ_∞ and Born effective charges Z_{eff} needed to compute LO/TO splitting at the Γ -point, are calculated using density functional perturbation theory as implemented in VASP by means of the Sternheimer equation (Gajdos et al., 2006; Baroni and Resta, 1986; Sternheimer, 1954). For these calculations, a primitive fcc unit cell and an $8 \times 8 \times 8$ Monkhorst and Pack (1976) \mathbf{k} -point grid is used.

Table 1

Summary of FPMD simulations from which phonon lifetimes and anharmonic frequencies are determined. Uncertainties are at most 3 K for T and 1.5 GPa for P .

| ρ (g/cm ³) | T (K) | P (GPa) |
|--------------------------------|------------|--------------|
| <i>2×2×2 simulation cells</i> | | |
| 3.37 | 965 | −3.2 |
| | 1004 | −2.9 |
| | 2027 | 3.6 |
| 3.67 ^a | 680 | 6.6 |
| | 1180 | 9.8 |
| | 1530 | 12.0 |
| | 1860 | 14.0 |
| | 2350 | 17.2 |
| 3.75 | 630 | 10.8 |
| | 1540 | 16.5 |
| | 1903 | 19.0 |
| 4.05 | 1034 | 30.9 |
| | 1825 | 36.3 |
| | 2551 | 40.9 |
| 4.46 | 1396 | 63.9 |
| | 1759 | 66.2 |
| | 2101 | 68.3 |
| 4.76 | 990 | 89.7 |
| | 1750 | 94.8 |
| | 2485 | 99.6 |
| 5.10 | 505 | 123.5 |
| | 1850 | 133.1 |
| | 2795 | 139.7 |
| 5.49 | 817 | 175.2 |
| | 1671 | 181.6 |
| | 2238 | 185.6 |
| | 3505 | 195.2 |
| <i>3×3×3 simulation cells</i> | | |
| 3.67 ^a | 957 | 8.2 |
| 5.49 | 1238 | 198.6 |

^a Simulations of de Koker, 2009.

4. Thermal conductivity of MgO periclase

Phonon lifetimes determined for each vibrational mode (Fig. S1) are generally consistent with the $1/T$ dependence predicted in Eq. (7). Vibrational frequencies corresponding to each of these points are in close agreement with the harmonic frequencies computed from the force constant matrix (Fig. S2); group velocities computed from harmonic frequencies therefore give an accurate representation of the true anharmonic case. Computed values of the dielectric constant and Born effective charges used in obtaining the harmonic frequencies are reported in Table 2.

Thermal conductivity values computed from these lifetimes and frequencies are shown in Fig. 1. Computational results agree closely with the available experimental data (Goncharov et al., 2009; Katsura,

Table 2

Dielectric constants ϵ_∞ and Born effective charges Z_{eff} computed for MgO periclase.

| ρ (g/cm ³) | This study | | Previous estimates | |
|--------------------------------|-------------------|------------------|---|---------------------------------------|
| | ϵ_∞ | Z_{eff} | ϵ_∞ | Z_{eff} |
| 3.37 | 3.19 | 1.97 | 3.18 ^a | 1.95 ^a |
| 3.67 | 3.10 | 1.94 | 3.15 ^a , 3.10 ^b , 3.01 ^c | 1.94 ^a , 1.93 ^b |
| 3.75 | 3.08 | 1.93 | 3.07 ^a | 1.93 ^a |
| 4.05 | 3.00 | 1.90 | 2.99 ^a | 1.89 ^a |
| 4.46 | 2.93 | 1.86 | 2.91 ^a | 1.86 ^a |
| 4.76 | 2.90 | 1.83 | 2.88 ^a | 1.84 ^a |
| 5.10 | 2.87 | 1.81 | 2.83 ^a | 1.81 ^a |
| 5.49 | 2.85 | 1.78 | 2.83 ^a | 1.79 ^a |

^a Oganov et al., 2003.

^b Karki et al., 2000.

^c Jasperse et al., 1964.

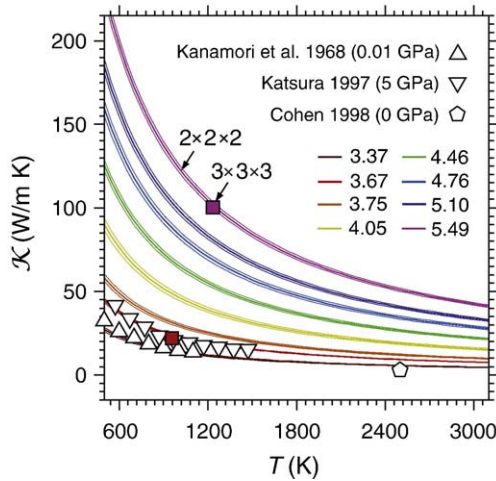


Fig. 1. Lattice thermal conductivity of MgO periclase computed via equilibrium first-principles molecular dynamics. Lines give results from computations with $2 \times 2 \times 2$ supercells, squares results for $3 \times 3 \times 3$ supercells, colored according to density. Conductivity results are in very close agreement with the experimental data of Kanamori et al. (1968), Katsura (1997), and Goncharov et al. (2009) (see Fig. 2), and is also similar to the previous theoretical result of Cohen (1998).

1997; Kanamori et al., 1968). Thermal conductivity is seen to increase strongly upon compression, due both to the increase in phonon group velocities that result from higher vibrational frequencies (Fig. S2), and to the increase in phonon lifetimes (Fig. 2, inset). Increasing phonon lifetimes imply longer mean free path lengths; since a denser structure would rather shorten mean free paths (Hofmeister, 2007), this indicates a notable decrease in anharmonicity with compression.

Due mostly to the large difference in mean group velocity between the acoustic and the optic modes, as well as the fact that lifetimes of optic modes are shorter than acoustic modes by roughly a factor of two, acoustic modes contribute $\sim 95\%$ to phonon conductivity at all

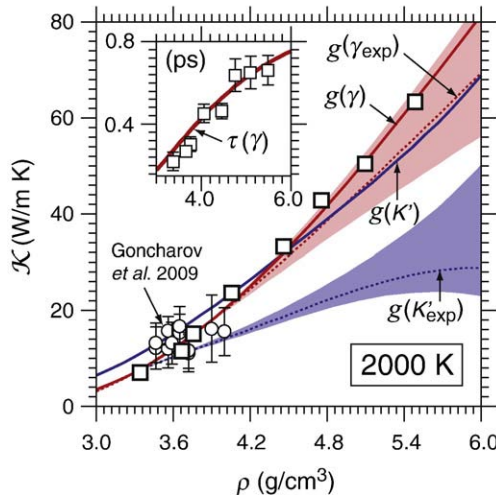


Fig. 2. Computed lattice thermal conductivities at 2000 K (squares), compared to fits (solid lines) and extrapolations (dotted lines with uncertainty envelopes) of Eq. (17) with $g(\gamma)$ as given by Eq. (12) (red curves) and $g(K'_T)$ as in Eq. (16) (blue curves). Fitted models use the FPMD based self consistent thermodynamic model for MgO of de Koker and Stixrude (2009); extrapolations use experimental data for the Grüneisen parameter and equation of state (see text). Computed conductivity results agree closely with the experimental data of Goncharov et al. (2009). Inset: effective phonon lifetimes at 2000 K in picoseconds, computed from the mean A values (Fig. S1) as $\tau = 1/AT\nu_D^2$, ν_D being the characteristic Debye frequency at each density. The line indicates the fit of Eq. (10) to these values.

densities considered. The dominant role of acoustic modes in lattice conductivity has a very important implication: the Debye approximation to the kinetic transport equation (Eq. (6)) will give an excellent representation of conductivity in simple oxides, and likely also captures conductive transport in more complex silicate structures quite accurately.

Combining our conductivity results with the FPMD-derived fundamental thermodynamic relation for MgO periclase of de Koker and Stixrude (2009) yields a complete, internally consistent set of physical properties. We use this set to test the extent to which the variation of lattice conductivity with density can be expressed in terms of more readily determined thermodynamic parameters, such as the equation of state and the Grüneisen parameter. We consider two such expressions: the first is that derived from Debye theory (Eq. (12)), which requires a description of $\gamma(\rho)$, i.e. implicit knowledge of the anharmonicity in the material; the second is that given in Eq. (16), which requires a description of $K'_T(\rho)$, i.e. knowledge only of the equation of state. In both these descriptions κ_0 is the only adjustable parameter, which we determine by minimizing the misfit between the two respective models for $\kappa(\rho)$ and our results (Fig. 2), with $\gamma(\rho)$ and $K'_T(\rho)$ taken from the FPMD study of de Koker and Stixrude (2009). To assess the extent to which ambient pressure conductivity values can be extrapolated to high pressure using experimental Grüneisen parameter and/or equation of state data, we also consider $\kappa(P)$ models constructed using our lowest density conductivity computation as reference value (κ_0), together with experimental estimates for $\gamma(\rho)$ and $K'_T(\rho)$ (Stixrude and Lithgow-Bertelloni, 2007; Stixrude and Lithgow-Bertelloni, 2005; Speziale et al., 2001; Duffy and Ahrens, 1995; Fei, 1995).

As seen in Fig. 2, the fit of Eq. (12) to our computed κ results is notably superior to the fit of Eq. (16). This difference is highlighted further in the experimental extrapolations: the model based on Eq. (12) follows the computed conductivities to within experimental uncertainty, yet that based on Eq. (16) underestimates κ by nearly a factor of two. The parameters for our preferred model of the density and temperature dependence of the conductivity of periclase are reported in Table 3. $\kappa(P)$ isotherms for this model are shown in Fig. 3a, together with the thermal conductivity along a model geotherm (Fig. 4a, see below), and along the FPMD-derived principle Hugoniot and the melting curves for MgO periclase computed by (de Koker and Stixrude 2009).

It is therefore clear that, even for a simple oxide such as MgO periclase, knowledge only of the equation of state is not sufficient to extrapolate low pressure conductivity measurements to the lower mantle. Conversely, $\gamma(\rho)$ is sufficiently well known for almost all major mantle phases that the pressure dependence of their lattice conductivity may be represented via Eq. (12) (e.g. Xu et al., 2008; Stixrude and Lithgow-Bertelloni, 2005).

5. Geophysical implications

Thermal conductivity at the base of the lower mantle is a key physical property, crucial to our understanding of the thermal state and evolution of both the mantle and the core. By constraining the amount of heat leaving the core, it plays a central role in the thermal evolution of the entire planet, influencing for example the age of the inner core (Labrosse, 2003; Buffett et al., 1992), the possible presence of radiogenic isotopes in the core (Davies, 2007; Nimmo et al., 2004; Buffett, 2002; Gessman and Wood, 2002), and the nature of heat sources for the development of instabilities associated with mantle plumes (Zhong, 2006). Together with the lateral temperature distribution at the base of the mantle, it acts as a key boundary constraint in the generation of the magnetic field (Sakuraba and Roberts, 2009; Buffett, 2009; Glatzmaier and Roberts, 1995).

Attempts have been made to estimate the core–mantle boundary heat flux from seismic estimates of the thermal gradient and

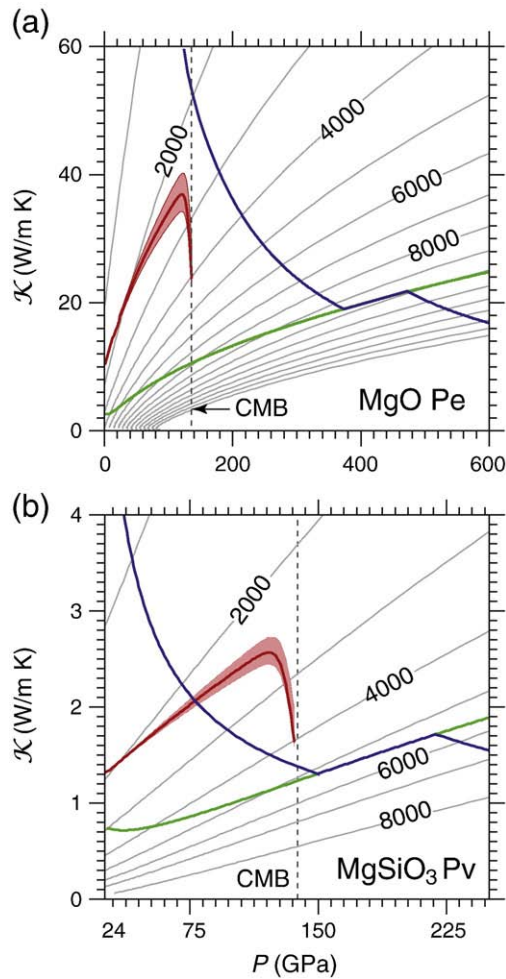


Fig. 3. Lattice thermal conductivity of (a) MgO periclase and (b) MgSiO₃ perovskite along isotherms (grey lines), the model geotherm shown in Fig. 4a (red line and uncertainty envelope), and along the FPMD based principal Hugoniot (blue line) and melting curves (green line) of de Koker and Stixrude (2009), computed using parameters in Table 3.

experimental extrapolations of κ in the lower mantle (Goncharov et al., 2009; Buffett, 2007; Hernlund et al., 2005). Although such estimates are rather approximate in the light of lateral variations in thickness, chemistry and temperature of the boundary layer, they do give crucial first order information on the nature of heat transport in the region. Having a robust model of the variation of κ with pressure, temperature, and composition can certainly contribute towards improving the accuracy and reliability of such estimates.

Based on our knowledge of phase equilibria and seismic properties of a primitive mantle composition at deep mantle pressures, the lower mantle is believed to consist dominantly of (Fe,Mg)O ferropericlase, (Fe,Mg)SiO₃ perovskite and CaSiO₃ perovskite in proportions of close to 20:73:7 (e.g. Stixrude and Lithgow-Bertelloni, 2007; Stixrude and Lithgow-Bertelloni, 2005). If we assume that the lattice conductivities of CaSiO₃ and (Fe,Mg)SiO₃ perovskite are similar, and that the decreasing effect on conductivity due to Fe in MgO periclase and Fe + Al in MgSiO₃ perovskite is balanced by the additional contribution from radiative conductivity, we may represent the bulk lattice conductivity of the lower mantle as a 20:80 proportional mixing of the lattice conductivities of MgO periclase and MgSiO₃ perovskite.

We represent the mantle geotherm using an adiabatic temperature gradient computed for a pyrolytic mantle composition with potential temperature of 1600 K (Stixrude and Lithgow-Bertelloni, 2007). To allow for lateral heterogeneity (e.g. Oganov et al., 2001) and a

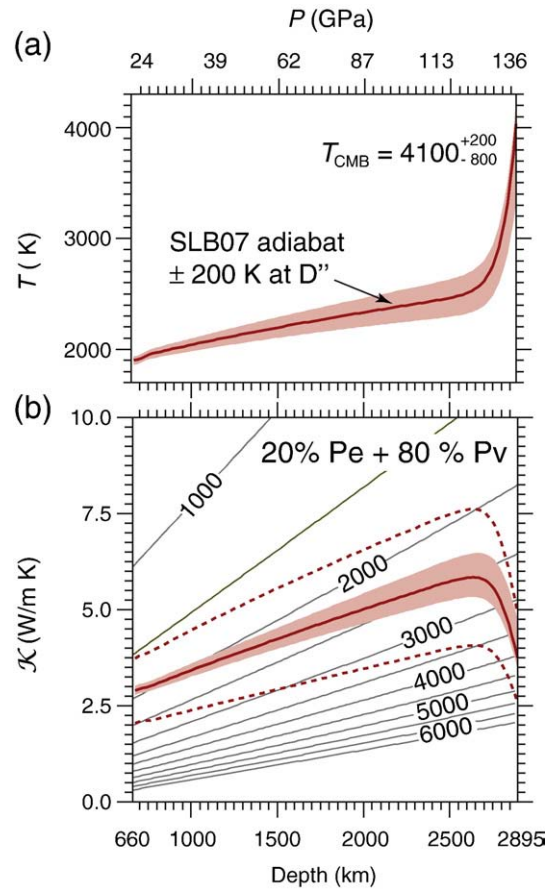


Fig. 4. (a) Model geotherm for the lower mantle, computed as an adiabat for a pyrolytic composition and a potential temperature of 1600 K with the model of Stixrude and Lithgow-Bertelloni (2007, 2005). An uncertainty of ± 200 K at the top of the thermal boundary layer is included to allow lateral heterogeneity and for sub-adiabaticity (see text). The range of temperatures at the top of the outer core is based on various estimates of the freezing point and adiabatic temperature profile of the liquid outer core (Alfè, 2009; Steinle-Neumann et al., 2001; Boehler, 2000; Brown and McQueen, 1986). (b) Thermal conductivity of the lower mantle along the model geotherm, computed as a 20:80 proportion Hashin–Shtrikman mixture of MgO periclase and MgSiO₃ perovskite. Solid lines denote mixing averages (thin – isotherms; thick – geotherm), dashed lines denote the upper and lower bounds. Pressure–depth conversion is based on the global seismic model PREM (Dziewonski and Anderson, 1981).

reasonable extent of convective sub-adiabaticity (e.g. Schuberth et al., 2008), we include an uncertainty of ± 200 K at the top of the thermal boundary layer. The temperature at the top of the outer core is taken as 4100^{+200}_{-800} K, consistent with various estimates of the freezing point and adiabatic temperature profile of liquid Fe at core pressures (Alfè, 2009; Steinle-Neumann et al., 2001; Boehler, 2000; Brown and McQueen, 1986).

To account for the lattice conductivity of MgSiO₃ perovskite in the deep mantle, we extrapolate the ambient pressure measurements of Osako and Ito (1991) using the first-principles thermodynamic model for MgSiO₃ perovskite of de Koker and Stixrude (2009). Parameters used in this extrapolation are reported in Table 3. $\kappa(P)$ isotherms together with κ along the model geotherm and along the FPMD-derived principle Hugoniot and melting curves for MgSiO₃ perovskite computed by de Koker and Stixrude (2009) are shown in Fig. 3b.

The subsequent bulk lattice conductivity of a randomly oriented aggregate of 20% periclase and 80% perovskite (Hashin–Shtrikman average; Fig. 4b) at the top of the thermal boundary layer is found to be 5.9 ± 0.6 W/m K, with a value of 4.0 ± 0.5 W/m K at the base. These estimates of κ at the core–mantle boundary are somewhat lower than the Debye theory based extrapolation of Goncharov et al. (2009), because the aggregate mean in that study was computed simply as the

Table 3

Parameters of preferred lattice conductivity models, as described in Eqs. (12)–(17). γ_0 and q_0 are based on results of de Koker and Stixrude, 2009.

| | ρ_0 | T_0 | \mathcal{K}_0 | γ_0 | q_0 |
|--------------------|----------|-------|------------------|------------|-------|
| MgO | 3.30 | 2000 | 7.01 | 1.49 | 1.27 |
| MgSiO ₃ | 3.87 | 2000 | 0.7 ^a | 1.73 | 1.58 |

^a Osako and Ito (1991).

weighted arithmetic mean (i.e. the Voigt mixing upper bound). Comparison to the analysis of Goncharov et al. (2009) indicates that our Hashin–Strikman aggregate mean corresponds to a core–mantle boundary heat flux of about 3–4 TW, at the lower end of the various geophysics based estimates (e.g. Lay et al., 2008). This allows a notable amount of space for our assumption that radiative conductivity is small to be relaxed: as improved constraints on the radiative conductivity of lower mantle minerals become available, our models for lattice $\mathcal{K}(\rho, T)$ of periclase and perovskite can be readily supplemented to determine the bulk $\mathcal{K}(P, T)$ for the lowermost mantle.

6. Conclusion

Using a combination of first-principles molecular dynamics and first-principles lattice dynamics methods, we have calculated the lattice thermal conductivity for MgO periclase over a range of pressures and temperatures applicable to the entire mantle. The results show that low pressure conductivity measurements can be reliably extrapolated to pressures characteristic of the lowermost mantle using Debye theory and knowledge of the density dependence of the Grüneisen parameter. This finding implies a notable decrease in the current range of uncertainty for values of lower mantle conductivity, potentially placing tighter constraints on the possible scenarios put forward for the thermal evolution of the core with associated generation of the magnetic field, as well as for the thermal state of the lower mantle.

Acknowledgements

This research was supported by the European Union under contract number MRTN-CT-2006-035957, and by the Deutsche Forschungsgemeinschaft under contract number KO 3958/1-1. Computing facilities were provided by the Leibniz Supercomputing Center of the Bavarian Academy of Sciences and Humanities. I am grateful to Stephen Stackhouse, Gerd Steinle-Neumann and Lars Stixrude for valuable input. Artem Oganov and an anonymous reviewer provided insightful comments on the manuscript.

Appendix A. Supplementary data

Supplementary data associated with this article can be found, in the online version, at doi:10.1016/j.epsl.2010.02.011.

References

Alfè, D., 2009. Temperature of the inner-core boundary of the Earth: melting of iron at high pressure from first-principles coexistence simulations. *Physical Review B* 79 R. Anderson, O.L., 1974. The determination of the volume dependence of the Grüneisen parameter γ . *J. Geophys. Res.* 79, 1153–1155.
 Baroni, S., Resta, R., 1986. Ab initio calculation of the macroscopic dielectric constant in silicon. *Physical Review B* 33, 7017–7021.
 Boehler, R., 2000. High-pressure experiments and the phase diagram of lower mantle and core materials. *Rev. Geophys.* 38, 221–245.
 Brown, J.M., 1986. Interpretation of the D'' zone at the base of the mantle: dependence on assumed values of thermal conductivity. *Geophys. Res. Lett.* 13, 1509–1512.
 Brown, J.M., McQueen, R.G., 1986. Phase transitions, Grüneisen parameter, and elasticity for shocked iron between 77 GPa and 400 GPa. *J. Geophys. Res.* 91, 7485–7494.
 Buffett, B.A., 2002. Estimates of heat flow in the deep mantle based on the power requirements for the geodynamo. *Geophys. Res. Lett.* 29. doi:10.1029/2001GL014649.

Buffett, B.A., 2007. A bound on heat flow below a double crossing of the perovskite–postperovskite phase transition. *Geophys. Res. Lett.* 34. doi:10.1029/2007GL030930.
 Buffett, B.A., 2009. Onset and orientation of convection in the inner core. *Geophysical Journal International* 173. doi:10.1111/j.1365-246X.2009.04311.x.
 Buffett, B.A., Huppert, H., Lister, J.R., Woods, A.W., 1992. Analytical model for the solidification of the Earth's core. *Nature* 356, 329–331.
 Burke, K., Steinberger, B., Torsvik, T.H., Smethurst, M.A., 2008. Plume generation zones at the margins of large low shear velocity provinces on the core–mantle boundary. *Earth Planet. Sci. Lett.* 265, 49–60.
 Ceperley, D.M., Alder, B.J., 1980. Ground-state of the electron–gas by a Stochastic method. *Phys. Rev. Lett.* 45, 566–569.
 Cohen, R., 1998. Thermal conductivity of MgO at high pressures. *Review of High Pressure Science and Technology* 7, 160–162.
 Davies, G.F., 2007. Mantle regulation of core cooling: a geodynamo without core radioactivity? *Phys. Earth Planet. In.* 160, 215–229.
 de Koker, N., 2009. Thermal conductivity of MgO periclase from equilibrium first principles molecular dynamics. *Phys. Rev. Lett.* 103. doi:10.1103/PhysRevLett.103.125902.
 de Koker, N., Stixrude, L., 2009. Self-consistent thermodynamic description of silicate liquids, with application to shock melting of MgO periclase and MgSiO₃ perovskite. *Geophysical Journal International* 178, 162–179.
 de Koker, N., Stixrude, L., Karki, B.B., 2008. Thermodynamics, structure, dynamics, and freezing of Mg₂SiO₄ liquid at high pressure. *Geochim. Cosmochim. Acta* 72, 1427–1441. doi:10.1016/j.gca.2007.12.019.
 Duffy, T.S., Ahrens, T.J., 1995. Compressional sound velocity, equation of state, and constitutive response of shock-compressed magnesium oxide. *J. Geophys. Res.* 100, 529–542.
 Dziewonski, A.M., Anderson, D.L., 1981. Preliminary reference Earth model. *Phys. Earth Planet. In.* 25, 297–356.
 Fei, Y., 1995. Thermal expansion. In: Ahrens, T.J. (Ed.), *Mineral Physics and Crystallography: A Handbook of Physical Constants, Volume 2*. American Geophysical Union, Washington, D.C, pp. 29–44. AGU Reference Shelf.
 Gajdos, M., Hummer, K., Kresse, G., J. F., F. B., 2006. Linear optical properties in the PAW methodology. *Physical Review B* 73, 045112.
 Gessman, C.K., Wood, B.J., 2002. Potassium in the Earth's core? *Earth Planet. Sci. Lett.* 200, 63–78.
 Glatzmaier, G.A., Roberts, P.H., 1995. A three dimensional convective dynamo solution with rotating and finitely conducting inner core and mantle. *Phys. Earth Planet. In.* 91, 63–75.
 Goncharov, A.F., Beck, P., Struzhkin, V.V., Haugen, B.D., Jacobsen, S.D., 2009. Thermal conductivity of lower-mantle minerals. *Phys. Earth Planet. In.* 174, 24–32.
 Goncharov, A.F., Haugen, B.D., Struzhkin, V.V., Beck, P., Jacobsen, S.D., 2008. Radiative conductivity in the Earth's lower mantle. *Nature* 456, 231–234.
 Hernlund, J.W., Thomas, C., Tackley, P.J., 2005. A doubling of the post-perovskite phase boundary and structure of the Earth's lowermost mantle. *Nature* 343, 882–886.
 Hofmeister, A.M., 1999. Mantle values of thermal conductivity and the geotherm from phonon lifetimes. *Science* 283, 1699–1706.
 Hofmeister, A.M., 2007. Pressure dependence of thermal transport properties. *Proc. Natl. Acad. Sci.* 104, 9192–9197.
 Hofmeister, A.M., Yuen, D.A., 2007. Critical phenomena in thermal conductivity: implications for lower mantle dynamics. *Journal of Geodynamics* 44, 186–199.
 Hohenberg, P., Kohn, W., 1964. Inhomogeneous electron gas. *Physical Review* 136, 864–871.
 Jasperse, J.R., Kahan, A., Plendl, J.N., Mitra, S.S., 1964. Temperature dependence of infrared dispersion in ionic crystals of LiF and MgO. *Physical Review* 146, 526–542.
 Julian, C.L., 1965. Theory of heat conduction in rare-gas crystals. *Physical Review* 137, 128–137.
 Kanamori, H., Fujii, N., Mizutani, H., 1968. Thermal diffusivity measurement of rock-forming minerals from 300° to 1100°K. *J. Geophys. Res.* 73, 595–605.
 Karki, B.B., Wentzcovitch, R.M., De Gironcoli, S., Baroni, S., 2000. High-pressure lattice dynamics and thermoelasticity of MgO. *Physical Review B* 61, 8793–8800.
 Katsura, T., 1997. Thermal diffusivity of periclase at high temperatures and pressures. *Phys. Earth Planet. In.* 101, 73–77.
 Keppler, H., Dubrovinsky, L.S., Narygina, O., Kantor, I., 2008. Optical absorption and radiative thermal conductivity of silicate perovskite to 125 gigapascals. *Science* 322, 1529–1532.
 Kieffer, S.W., 1976. Lattice thermal conductivity within the earth and considerations of a relationship between the pressure dependence of the thermal diffusivity and the volume dependence of the Grüneisen parameter. *J. Geophys. Res.* 81, 3025–3030.
 Klemens, P.G., 1958. Thermal conductivity and lattice vibrational modes. In: Seitz, F., Turnbull, D. (Eds.), *Solid State Physics, Volume 7*. Academic Press Inc, New York, pp. 1–98.
 Kohn, W., Sham, L.J., 1965. Self-consistent equations including exchange and correlation effects. *Physical Review* 140, 1133.
 Kresse, G., Furthmüller, J., 1996. Efficiency of ab-initio total energy calculations for metals and semiconductors using a plane-wave basis set. *Comput. Mater. Sci.* 6, 15–50.
 Kresse, G., Hafner, J., 1994. Norm-conserving and ultrasoft pseudopotentials for first-row and transition-elements. *Journal of Physics – Condensed Matter* 6, 8245–8257.
 Labrosse, S., 2003. Thermal and magnetic evolution of the Earth's core. *Phys. Earth Planet. In.* 140, 127–143.
 Lay, T., Hernlund, J., Buffett, B.A., 2008. Core–mantle boundary heat flow. *Nature Geoscience* 1, 25–32.
 Lay, T., Williams, Q., Garnero, E.J., 1998. The core–mantle boundary layer and deep Earth dynamics. *Nature* 392, 461–468.
 Monkhorst, H.J., Pack, J.D., 1976. Special points for Brillouin-zone integrations. *Physical Review B* 13, 5188–5192.
 Nimmo, F., Price, G.D., Brodholt, J., Gubbins, D., 2004. The influence of potassium on core and geodynamo evolution. *Geophysical Journal International* 156, 363–376.
 Oganov, A.R., Brodholt, J.P., Price, G.D., 2001. The elastic constants of MgSiO₃ perovskite at pressures and temperatures of the Earth's mantle. *Nature* 411, 934–937.

- Oganov, A.R., Dorogokupets, P.I., 2003. All-electron and pseudopotential study of MgO: equation of state, anharmonicity, and stability. *Physical Review B* 67. doi:10.1103/PhysRevB.67.224110.
- Oganov, A.R., Gillian, M.J., Price, G.D., 2003. Ab initio lattice dynamics and structural stability of MgO. *J. Chem. Phys.* 118, 10,174–10,182.
- Osako, M., Ito, E., 1991. Thermal diffusivity of MgSiO₃ perovskite. *Geophys. Res. Lett.* 18, 239–242.
- Parlinski K. (2008) Phonon Software.
- Peierls, R., 1929. Zur kinetischen Theorie der Wärmeleitung in Kristallen. *Annalen der Physik* 3, 1055–1101.
- Ross, R.G., Anderson, P., Sundqvist, B., Bäckström, G., 1984. Thermal conductivity of solids and liquids under pressure. *Reports on Progress in Physics* 47, 1347–1402.
- Roufosse, M.C., Klemens, P.G., 1973. Thermal conductivity of complex dielectric crystals. *Physical Review B* 7, 5379–5386.
- Sakuraba, A., Roberts, P.H., 2009. Generation of a strong magnetic field using uniform heat flux at the surface of the core. *Nature Geoscience* 2, 802–805.
- Schubert, G., Turcotte, D.L., Olson, P., 2001. *Mantle Convection in the Earth and Planets*. Cambridge University Press, Cambridge.
- Schuberth, B., Bunge, H.P., Steinle-Neumann, G., Moder, C., Oeser, J., 2008. Thermal vs. elastic heterogeneity in high-resolution mantle circulation models with pyrolytic composition: high plume excess temperatures in the lowermost mantle. *Geochemistry, Geophysics, Geosystems* 10. doi:10.1029/2008GC002235.
- Speziale, S., Zha, C.S., Duffy, T.S., Hemley, R.J., Mao, H.K., 2001. Quasi-hydrostatic compression of magnesium oxide to 52 GPa: implications for the pressure–volume–temperature equation of state. *J. Geophys. Res.* 106, 515–528.
- Steinle-Neumann, G., Stixrude, L., Cohen, R.E., Gülseren, O., 2001. Elasticity of iron at the temperature of the Earth's inner core. *Nature* 413, 57–60.
- Sternheimer, R.M., 1954. Electronic polarizabilities of ions from the Hartree–Fock wave functions. *Physical Review* 96, 951–968.
- Stixrude, L., de Koker, N., Sun, N., Mookherjee, M., Karki, B., 2009. Thermodynamics of silicate liquids in the deep Earth. *Earth Planet. Sci. Lett.* 278.
- Stixrude, L., Lithgow-Bertelloni, C., 2005. Thermodynamics of mantle minerals – I. Physical properties. *Geophysical Journal International* 162, 610–632.
- Stixrude, L., Lithgow-Bertelloni, C., 2007. Influence of phase transformations on lateral heterogeneity and dynamics in Earth's mantle. *Earth Planet. Sci. Lett.* 263, 45–55.
- Williams, Q., Garnero, E.J., 1996. Seismic evidence for partial melt at the base of Earth's mantle. *Science* 273, 1528–1530.
- Xu, W., Lithgow-Bertelloni, C., Stixrude, L., 2008. The effect of bulk composition and temperature on mantle seismic structure. *Earth Planet. Sci. Lett.* 275, 70–79.
- Zhong, Z., 2006. Constraints on thermochemical convection of the mantle from plume heat flux, plume excess temperature, and upper mantle temperature. *J. Geophys. Res.* 111. doi:10.1029/2005JB003972.
- Ziman, J.M., 1960. *Electrons and Phonons*. Oxford University Press, Oxford.